THE JOURNAL OF BIOLOGICAL CHEMISTRY
Vol. 279, No. 26, Issue of June 25, pp. 27294–27301, 2004

Printed in U.S.A.

Structure of Mammalian Cytochrome P450 2B4 Complexed with 4-(4-Chlorophenyl)imidazole at 1.9-Å Resolution

INSIGHT INTO THE RANGE OF P450 CONFORMATIONS AND THE COORDINATION OF REDOX PARTNER BINDING*

Received for publication, March 25, 2004, and in revised form, April 16, 2004
Published, JBC Papers in Press, April 20, 2004, DOI 10.1074/jbc.M403349200

Emily E. Scott‡§¶, Mark A. White§‖, You Ai He‡, Eric F. Johnson, C. David Stout‡‡, and James R. Halpert‡**

*From the ‡Department of Pharmacology and Toxicology and the ‖Sealy Center for Structural Biology, University of Texas Medical Branch, Galveston, Texas 77555-1031, the Departments of **Molecular and Experimental Medicine and ‡‡Molecular Biology, The Scripps Research Institute, La Jolla, California 92037*

A 1.9-Å molecular structure of the microsomal cytochrome P450 2B4 with the specific inhibitor 4-(4-chlorophenyl)imidazole (CPI) in the active site was determined by x-ray crystallography. In contrast to the previous experimentally determined 2B4 structure, this complex adopted a closed conformation similar to that observed for the mammalian 2C enzymes. The differences between the open and closed structures of 2B4 were primarily limited to the lid domain of helices F through G, helices B′ and C, the N terminus of helix I, and the β_4 region. These large-scale conformational changes were generally due to the relocation of conserved structural elements toward each other with remarkably little remodeling at the secondary structure level. For example, the F′ and G′ helices were maintained with a sharp turn between them but are placed to form the exterior ceiling of the active site in the CPI complex. CPI was closely surrounded by residues from substrate recognition sites 1, 4, 5, and 6 to form a small, isolated hydrophobic cavity. The switch from open to closed conformation dramatically relocated helix C to a more proximal position. As a result, heme binding interactions were altered, and the putative NADPH-cytochrome P450 reductase binding site was reformed. This suggests a structural mechanism whereby ligand-induced conformational changes may coordinate catalytic activity. Comparison of the 2B4/CPI complex with the open 2B4 structure yields insights into the dynamics involved in substrate access, tight inhibitor binding, and coordination of substrate and redox partner binding.

Cytochromes P450 (P450)[1] are involved in steroidogenesis, fatty acid metabolism, synthesis of bile and retinoid acids, and production of plant toxins, but it is their function in the elimination of xenobiotics that has received the most attention. In mammals, xenobiotic metabolizing P450s play the central role in detoxification of hydrophobic drugs, carcinogens, and toxins by decreasing the lipid solubility of these chemicals and, thus, promoting excretion. In contrast to the strict substrate selectivity of classical enzymes, xenobiotic-metabolizing P450s can each bind and oxidize a set of substrates with distinct sizes, shapes, and stereochemical features. Although the variety of substrates binding to a given P450 is often broad, the oxidation of each is usually remarkably regiospecific and stereospecific.

Identification of the structural basis for the specific monooxygenation and binding of a diverse but select set of substrates has been a particularly challenging goal, which is an important prerequisite for understanding selective substrate oxidation. Although the diversity of substrates might suggest an easily accessible active site, initial structures of both soluble bacterial (1) and microsomal mammalian (2) P450s revealed active sites buried within the globular structure of the protein. A few recent bacterial structures, however, suggest a "lid" domain composed of helices F and G, the motion of which controls substrate entry (3–5). Protein flexibility has also been implicated in dictating the regiospecificity of oxidation once a substrate is present in the active site. Structures of mammalian P450 2C5 with different substrates have shown that specific regions of the protein alter their conformation in response to the ligand present (6, 7). Structures of P450 119 with different bound ligands have revealed flexibility in regions composing both the upper active site and a putative substrate access channel (8, 9). The most dramatic differences in P450 conformation were recently observed for P450 2B4. This structure revealed that the protein can adopt a wide open conformation, allowing direct transfer of substrates from the protein exterior to the active site. This open cleft was grossly similar to openings observed in a few recent bacterial P450 structures (4, 5) and was stabilized by dimerization of the protein, which occurs both in the crystals and in solution. In the symmetric homodimer, a portion of one molecule (helices F′–G′) partially fills the cleft of the second molecule, with His-226 forming an intermolecular coordinate bond to the sixth position of the heme iron. Although reversible at low protein concentrations,

* This work was supported by National Institutes of Health Grants GM20674 (to E. E. S.), GM31001 (to E. F. J.), and ES03619 (to J. R. H.), Center Grant ES06676 (to J. R. H.), and a grant from the Sealy and Smith Foundation. The Advanced Light Source is supported by the Director, Office of Science, Office of Basic Energy Sciences, Materials Sciences Division of the United States Department of Energy under contract number DE-AC03-76SF00098 at the Lawrence Berkeley National Laboratory. The costs of publication of this article were defrayed in part by the payment of page charges. This article must therefore be hereby marked "*advertisement*" in accordance with 18 U.S.C. Section 1734 solely to indicate this fact.

The atomic coordinates and structure factors (code 1SUO) have been deposited in the Protein Data Bank, Research Collaboratory for Structural Bioinformatics, Rutgers University, New Brunswick, NJ (http://www.rcsb.org/).

§ These two authors contributed equally to the described investigation.

¶ Present address and to whom correspondence should be addressed: Dept. of Medicinal Chemistry, University of Kansas, 1251 Wescoe Hall Dr., 4070 Malott Hall, Lawrence, KS 66045-7582. Tel.: 785-864-5559; Fax: 785-864-5326; E-mail: eescott@ku.edu.

[1] The abbreviations used are: P450, cytochrome P450; CPI, 4-(4-chlorophenyl)imidazole; FOM, figure of merit; PDB, Protein Data Bank; r.m.s., root mean square; SRS, substrate recognition site.

formation of this symmetric dimer is spontaneous at the high protein concentrations required for crystallization. This dimerization precluded investigation of the structural consequences of ligand binding in the P450 2B4 active site.

The present report describes modifications of both the protein and crystallization conditions to yield an x-ray structure of the P450 2B4 complexed with the specific inhibitor 4-(4-chlorophenyl)imidazole (CPI). This experimentally determined structure was significantly different from the previous open structure of 2B4 and revealed a closed conformation more similar to that observed for the mammalian 2C enzymes. The structural differences between the open and closed structures of 2B4 yielded insights into the control of substrate access and the structural changes involved in tight inhibitor binding as well as the coordination of substrate and redox partner binding.

EXPERIMENTAL PROCEDURES

Site-directed Mutagenesis, Expression, and Purification—2B4dH differs from the wild type protein by truncation and modification of the N-terminal transmembrane domain and the addition of a C-terminal His_4 tag as described (10). For the present studies, an additional H226Y mutation was incorporated using overlapping primers containing the underlined mutations (5′-C TCG GGC TTC CTA AAG TAC TTT CCT GGC ACG CAC-3′ and 5′-GTG CGT GCC AGG AAA GTA CTT TAG GAA GCC CGA G-3′) and the QuikChange® mutagenesis kit (Stratagene). P450 2B4dH(H226Y) was expressed and purified as described for 2B4dH (10). Briefly, protein expression was induced in *Escherichia coli* transformed with the vector pKK2B4dH(H226Y) by the addition of isopropyl-1-thio-β-D-galactopyranoside to δ-aminolevulinic acid-supplemented Terrific broth media. The cells were harvested by centrifugation and lysed. After ultracentrifugation in the presence of high salt and the detergent Cymal-5 (Anatrace), the supernatant was purified using metal-affinity chromatography and then ion-exchange chromatography. The final buffer contained 50 mM potassium phosphate, 20% glycerol, 1 mM EDTA, 0.2 mM dithiothreitol, and 500 mM NaCl.

Enzymatic Assay—7-Ethoxy-4-trifluoromethylcoumarin oxidation was assayed as described (11) with 2.5 pmol of P450, 10 pmol of NADPH-cytochrome P450 reductase, 5 pmol of cytochrome b_5, and 2.5–160 μM 7-ethoxy-4-trifluoromethylcoumarin. Kinetic values K_{cat}, n, and S_{50} values were calculated from the Hill equation using nonlinear regression analysis in SigmaPlot (Jandel Scientific).

Structure Determination—CPI was obtained from Maybridge Chemical Co. (Cornwall, England) and prepared as a concentrated stock solution in ethanol. CPI was added to the dilute purified protein in ~10-fold excess, and the complex was concentrated by using a centrifugal device. The 2B4/CPI complex was crystallized from 4-μl vapor diffusion hanging drops containing 0.23 mM 2B4dH(H226Y), 0.5 mM CPI, 2.4 mM Cymal-5, 400 mM NaCl, 7.5% polyethylene glycol 10,000, 50 mM phosphate-citrate (pH 4), 25 mM potassium phosphate (pH 7.4), 0.5 mM EDTA, 0.1 mM dithiothreitol, and 10% glycerol. The drops were equilibrated against 300 mM NaCl, 15% polyethylene glycol 10,000, and 100 mM phosphate-citrate (pH 4) at 18 °C. Crystals were briefly soaked in the mother liquor supplemented with 30% glycerol added as a cryoprotectant, followed by flash freezing in liquid N_2. In addition, a halide derivative was prepared by substituting NaI for NaCl in the cryoprotectant solution.

Initial data were collected on a native crystal to 2.8 Å using a Bruker M06-HX22 x-ray generator and a Smart 2k CCD area detector over 180° (0.1° oscillations, 100 K) and processed using Proteum (Bruker AXS). Data were collected on the NaI derivative to 3 Å using a Macscience M06XHF x-ray generator and a MacScience DIP2030H area detector over 60° (0.25° oscillations, 100 K) and processed using DENZO and SCALEPACK (12). High-resolution data were collected to 1.9 Å on a single crystal using beam line 5.0.2 of the Advanced Light Source >90° (0.2° oscillations, 100 K) using a Quantum-210 CCD detector (Area Detector Systems Corp.) and processed using MOSFILM (13) and Scala (14). X-ray diffraction statistics are shown in Table I.

The complex crystallized in a different space group ($P6_322$) than the original 2B4 dimer. The first 2B4 structure (PDB identification 1PO5) was used as a search model for molecular replacement using Molrep (14). Portions of the solution, including helices B′ through C and F through G, did not fit the model-phased density, necessitating their removal from the initial model.

The partial model was used to phase cross Fourier maps. The native anomalous difference map showed only one strong peak, which was at the iron position. The isomorphous difference map allowed the location of 12 iodine sites in the NaI derivative. The iron site and the 12 iodine sites were used as a starting model for a heavy atom search using SOLVE (15). SOLVE found two additional iodine sites for a total of 14 iodines. The electron density map produced by SOLVE, FOM 0.36, was sufficient to clearly trace most of the protein backbone and locate the inhibitor. RESOLVE (16) was then used to perform solvent flipping and phase extension. The experimentally phased electron density map produced by RESOLVE, FOM 0.66, was sufficient to complete the amino acid chain and place the inhibitor. CPI was modeled using Insight II (Acelerys). CPI was energy minimized, and stereochemical restraints were generated using the PRODRG web server (17).

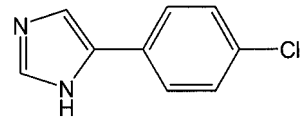

FIG. 1. **The structure of 4-(4-chlorophenyl)imidazole.**

The model was refined using CNS (18). Rigid body refinement was followed by iterative rounds of positional and isotropic variable σ B-factor (19) minimization until the R_{free} did not decrease, which was accomplished by using the PMB suite of structure refinement utilities. (The PMB suite is available from the author M. A. W. (www.x-ray.utmb.edu/PMB)). The structure factors were corrected for anisotropic scattering and absorption using a local scaling algorithm (20) incorporated into the PMB utilities. The Xfit module of Xtalview (21) was used for model building into the FOM-weighted experimental map and, later, the 1.9-Å σ_A-weighted $2|F_o| - |F_c|$ electron density maps.

Structure evaluation with PROCHECK (22) indicates that the final model has good stereochemistry with only two residues in disallowed regions (Lys-29 and Val-39) and one in a generously allowed region (Ser-430) of the Ramachandran plot. Lys-29 and Val-39 occur near the N terminus and are poorly defined. Ser-430 is well defined and also occurs as an outlier in the open 2B4 structure, which is likely related to its role in heme propionate binding and interactions near the proximal Cys-436 heme ligand. The atomic coordinates have been deposited in the PDB (1SUO).

RESULTS

Structure Determination of 2B4/CPI Complex—To investigate the conformation that 2B4 adopts when a ligand is bound, two approaches were used to inhibit the symmetric spontaneous homodimerization that occurs under the crystallization conditions that led to the previous 2B4 structure (10). First, to remove the stabilizing interaction between the imidazole nitrogen of His-226 and the heme iron, His-226 was mutated to a tyrosine residue. The 2B4dH(H226Y) protein had kinetic constants for the marker substrate 7-ethoxy-4-trifluoromethylcoumarin (k_{cat} = 13.3 min^{-1}, n = 1.3, S_{50} = 31.6 μM) that were very similar to those observed for 2B4dH (k_{cat} = 11.7 min^{-1}, n = 1.3, S_{50} = 28.5 μM). Second, a complex with the specific inhibitor CPI (Fig. 1) was formed prior to protein concentration for crystallization. CPI binds specifically and tightly to 2B4 with an IC_{50} of 0.04 μM (23). Binding of CPI to 2B4 wild type, 2B4dH, or 2B4dH(H226Y) results in an immediate shift of the Soret peak from 418 nm, characteristic of the low spin form, to 424 nm, characteristic of nitrogen ligation to the heme iron (data not shown).

The complex of CPI with 2B4dH(H226Y) crystallized in the $P6_322$ space group with a single molecule in the asymmetric unit. Although crystals could be obtained under similar conditions without the H226Y substitution, they were significantly more mosaic and, therefore, diffracted to a much lower resolution. Two initial lower resolution data sets were collected for 2B4dH(H226Y), one native (anomalous iron) and one iodine derivative. The structure was solved by molecular replacement using the native data set and the previous structure of P450 2B4dH (PDB identification 1PO5). The initial maps were easily interpreted for most of the protein, but large structural changes were more clearly confirmed by the experimental elec-

TABLE I
Data collection and refinement statistics

	Native	NaI derivative	High resolution
Crystal			
Space group	$P6_322$	$P6_322$	$P6_322$
Unit cell (Å)			
a	233.71	233.61	233.38
b	233.71	233.61	233.38
c	56.73	56.69	56.38
Data collection			
Wavelength (Å)	1.5418	1.5418	1.0001
Resolution range (Å)	56–2.8	50–3.0	49–1.9
Total observations	162,262	108,282	638,636
Unique observations	22,618	16,797	71,573
Completeness (%)	98.0 (88.0)[a]	88.9 (85.1)	99.9 (100)
Redundancy	7.2 (2.1)	6.4 (5.8)	8.9 (6.0)
I/σ_I	4.4 (0.9)	15.6 (7.5)	6.8 (1.3)
R_{merge} (%)	12.2 (38.1)	9.7 (21.7)	7.4 (55.3)
Phasing			
No. of sites	1	14	
FOM SOLVE/RESOLVE	0.36/0.66	0.36/0.66	N.A.[b]
Refinement statistics			
R-factor (%)			21.5
R_{free} (%)			23.9
r.m.s. deviations			
Bonds (Å)			0.017
Angles (°)			1.8
Model statistics		No. of atoms	Average *B*-factor (Å^2)
Protein		3735	47.6
Heme		43	47.8
CPI		12	33.4
Water		190	38.1

[a] Values for the highest resolution shell are in parentheses.
[b] N.A., not applicable.

tron density map from the single NaI derivative and anomalous iron. The majority of the model was built using this experimental electron density map. The final model was refined against data from a crystal diffracting to 1.9-Å resolution using iterative model adjustment and refinement. The final model is characterized by an *R* value of 21.5% and an R_{free} of 23.9% (Table I).

CPI Binding Results in a Conformational Change to Close the Cleft in P450 2B4dH—With CPI bound, the tertiary structure 2B4 adopts a conformation in which the inhibitor is tightly packed within the active site of the protein with no apparent entry or exit channel (Fig. 2). In general, the regions surrounding the open cleft observed in the original 2B4 structure have moved toward each other to isolate the bound inhibitor from the exterior of the protein. In the CPI complex, helices F through G cap the active site and interact with the N-terminal structures, the B′/C loop, the N terminus of helix I, and the β_4 system. The overall result is a P450 conformation more similar to the closed form observed for the mammalian P450s 2C5 (2, 6, 7), 2C8 (24), and 2C9 (25) (Fig. 3*A*) than the recent 2B4 open structure (Fig. 3*B*).

This large scale conformational change between the open and closed, or CPI-bound, structures of 2B4 occurs with strict conservation of the majority of the protein backbone. Whereas an alignment of the two 2B4 structures using all Cα atoms yields an r.m.s. deviation of 5.56 Å, alignment excluding four structurally divergent regions results in an r.m.s. deviation of only 1 Å, indicating that the remainder of the protein is remarkably unchanged. These four regions with the largest differences between the two 2B4 structures encompass helices B′ and C, helices F through G, the N terminus of helix I and the preceding loop, and the β_4 system (Fig. 3*B*). Remarkably little restructuring is required at the secondary structure level to generate the two very different conformations of 2B4 (Fig. 4).

The majority of the change in active site accessibility occurs because of the relocation of residues in the helix F through the helix G region. In contrast to the open 2B4 conformation, the CPI complex of 2B4 has an extra four-residue turn at the C terminus of the F helix (Figs. 4 and 5), altering the helix to end at the same position as the F helices of the closed 2C structures (Fig. 3*A*). The general position of the F helix is retained so that the additional turn extends the helix farther over the heme group. Although the CPI complex retains the short F′ and G′ helices observed in the 2B4 open structure (Fig. 4), they now extend over the active site (Fig. 5). In fact, residues in helix G′ of the CPI complex occupy space filled by B′ residues in the open conformation. As occurs in the open structure, there is a sharp bend between helices F′ and G′ at F220. The single internal mutation H226Y occurs at the C terminus of helix G′ and is exposed to solution with no side chain interactions that would be substantially modified by the substitution. Although the secondary structure of helix G is also largely conserved, it forms a much more acute angle over helix I in the CPI complex (Fig. 5). This pivoting of helix G on its C terminus results in the extension of its N terminus farther over the active site to partially close the cleft observed in the open conformation of 2B4.

The accessibility of the active site is also significantly altered by the organization and placement of the region including helix B′ through the C/D loop. The short B′ helix is flanked by two G*X*G motifs (Fig. 4). In the open 2B4 structure, helix B′ is divorced from helix G by >15 Å; but in the CPI complex, residues of helix B′ and the encompassing B/C loop interact with multiple residues in helices F′ and G (Fig. 5). The majority of the residues between these two G*X*G motifs satisfy all hydrogen bonds internally or to exterior water molecules. Thus, interactions between the tip of the B/C region, including the B′ helix, and the rest of the protein primarily involve van der Waals forces. In addition, the structure of the CPI complex reveals that the C helix is pivoted on its C terminus toward the proximal side of the protein (Fig. 5) and that the C/D loop is four residues longer (Fig. 4), features that are similar to the characteristics of these two elements in other closed P450 structures. The longer C/D loop includes a third flexible G*X*G motif that allows the shift in the C helix while retaining the

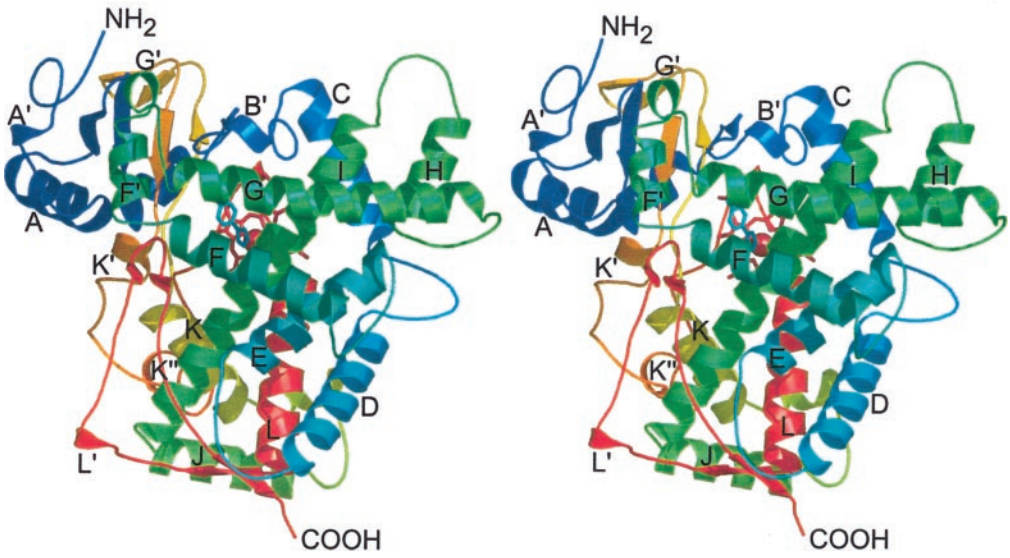

FIG. 2. **Divergent (walleye) stereo view of cytochrome P450 2B4dH(H226Y) with CPI bound.** The sequence can be traced from the *blue* N terminus to the *red* C terminus. Major helices and termini are labeled. Heme and CPI are shown in *red* and *cyan sticks*, respectively. Images generated using PyMOL (www.pymol.org) (41) unless otherwise credited.

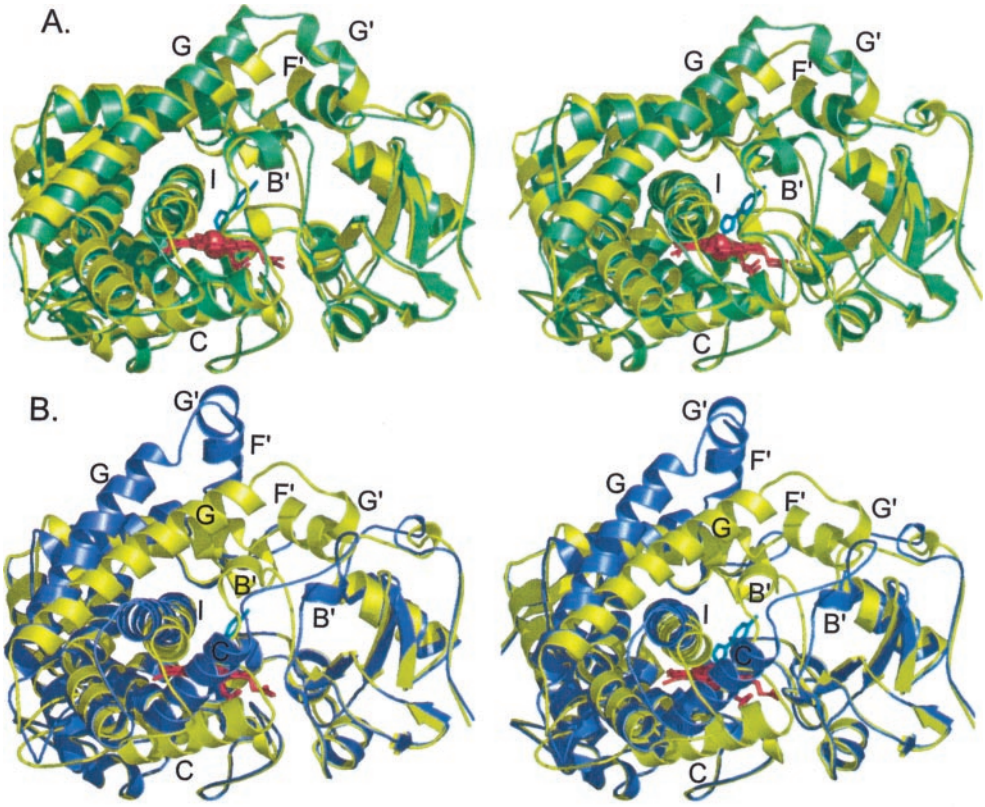

FIG. 3. **Comparison of the 2B4/CPI complex with other P450 structures.** *A*, divergent (walleye) stereo view of the 2B4/CPI structure (PDB 1SOU, *yellow*) superimposed on the 2C8 (PDB 1PQ2, *green*) structure. Structures were aligned by the conserved tertiary structure (2B4 numbered residues 29–99, 106–136, 140–216, 221–225, 241–249, 262–471, and 476–491; r.m.s. deviation 1.30 Å). *B*, divergent (walleye) stereo view of the open 2B4 structure (PDB 1PO5, *blue*) superimposed on the 2B4/CPI structure (*yellow*). The structures were aligned by the conserved tertiary structure (residues 28–99, 141–202, 263–275, 291–473, and 480–492; r.m.s. deviation 1 Å). Structural alignments were generated using Swiss PDB Viewer (42). The heme and CPI are shown in *red* and *cyan* sticks, respectively. Major helices whose placement differ between 2B4 and 2B4/CPI are labeled.

location of helix D. The first G*X*G motif preceding the B′ helix (residues Gly-97 to Gly-99) and the third motif in the C/D loop (Gly-136 to Gly-138) allow the conformations of 2B4 to diverge significantly between these two flex points but permit conservation of the structures just beyond them (Fig. 5).

The cleft of the open 2B4 structure is also partially closed by a straightening of the N-terminal half of helix I. In the open conformation, helix I forms a significant bend that originates at Gly-299 as the helix passes over the heme, whereas helix I of the CPI complex is much straighter (Fig. 5). As a result, the helix I backbone has moved by >4.5 Å at its N terminus. Both helices maintain the non-canonical helical turn adjacent to Thr-302 and two intervening water molecules predicted to be involved in catalysis. The conformation of the N terminus of

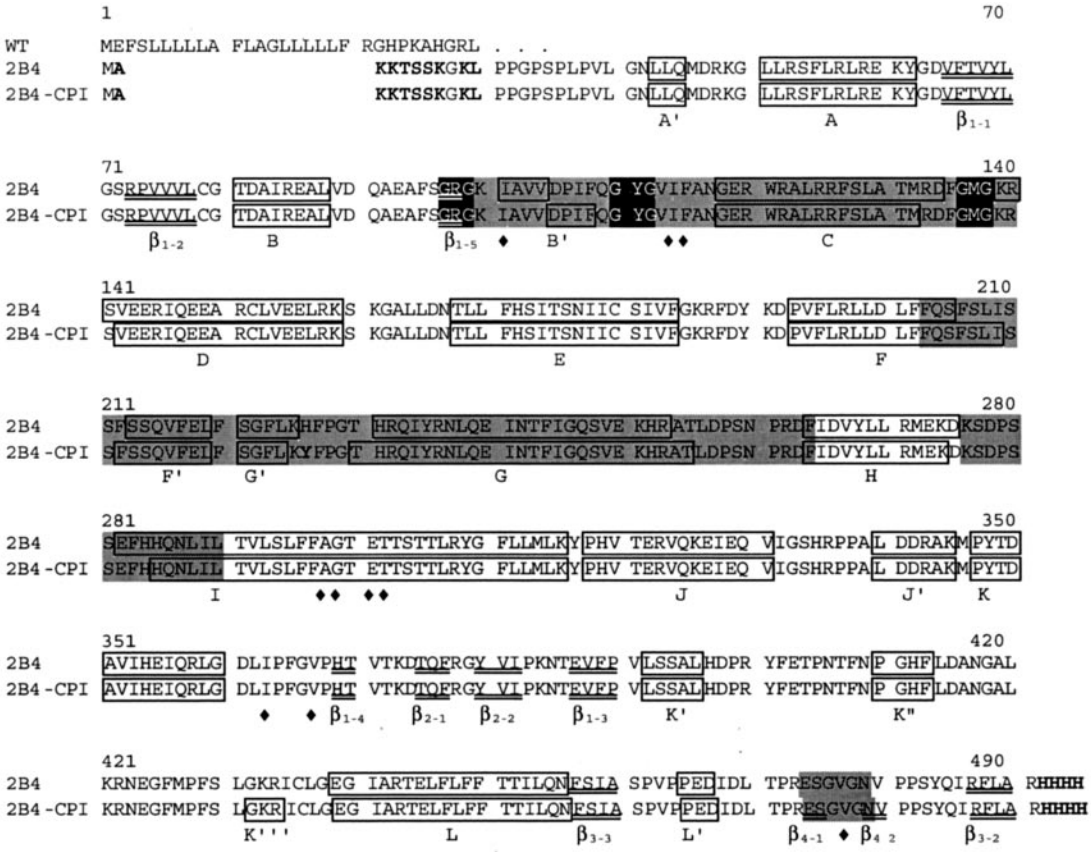

FIG. 4. **Secondary structure of the open and closed conformations of 2B4.** *Boxes* and *double underlines* represent helices and β sheets, respectively. The four regions with the highest r.m.s. deviations between the two 2B4 structures are *shaded*. Mutations are shown in *boldface*. The three G*X*G motifs are identified by *reversed text*. Residues that interact with CPI are indicated by *diamonds* below the sequence.

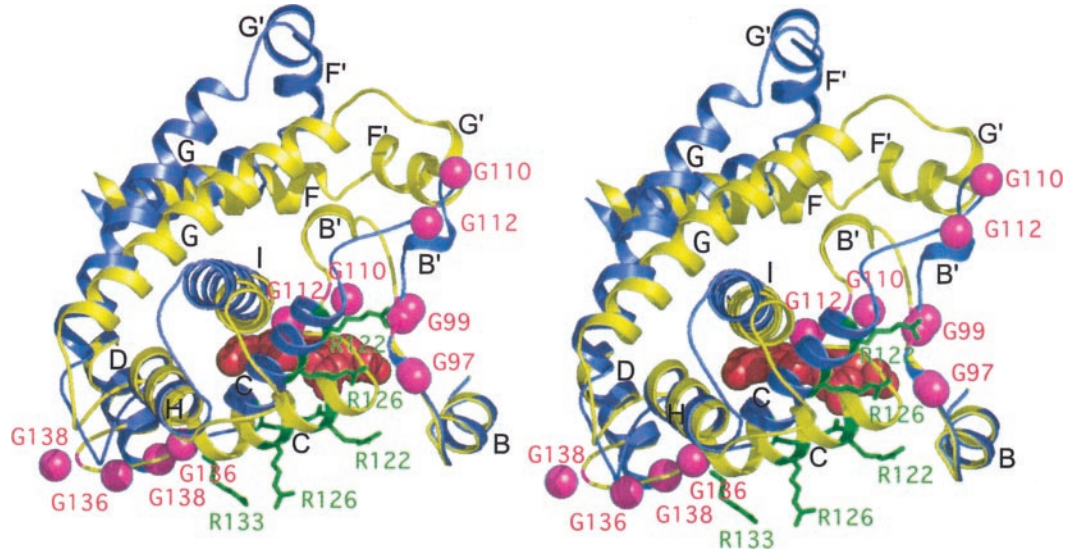

FIG. 5. **Spatial relationships between dynamic elements of the 2B4 (*blue*) and 2B4/CPI (*yellow*) structures shown in divergent (walleye) stereo.** The B/C loop and helix C are flanked by G*X*G motifs. The Cα atoms of these glycine residues are shown as *magenta spheres* and labeled. The G/H and C/D loops interact on the proximal face of the protein. Interactions with other dynamic elements and the flexibility of the B/C and C/D loops reposition the C helix residues involved in redox partner binding (*green sticks*).

helix I is likely influenced by alterations in helices G and C, as all three structural elements appear to be repositioned along the same vector (Fig. 5). The loop between helix H and the N terminus of helix I appears to be a flexible linker, as helix H is similarly placed in both 2B4 conformations. In the CPI complex, this H/I loop is extended by four residues, primarily at the expense of a partial turn of helix I present in the open conformation (Fig. 4).

On the opposite side of the F′/G′ region from the N-terminal I helix is the β_4 system. In the CPI complex, two two-residue β-sheets form the sides of a sharp turn that extends toward helix F (Fig. 2). This contrasts with the open conformation, where the β-sheet system is disordered and the tip of the loop is deflected away from helix F to open up a portion of the putative substrate access cleft.

Inhibitor Binding Site—The $2|F_o| - |F_c|$ maps revealed clear

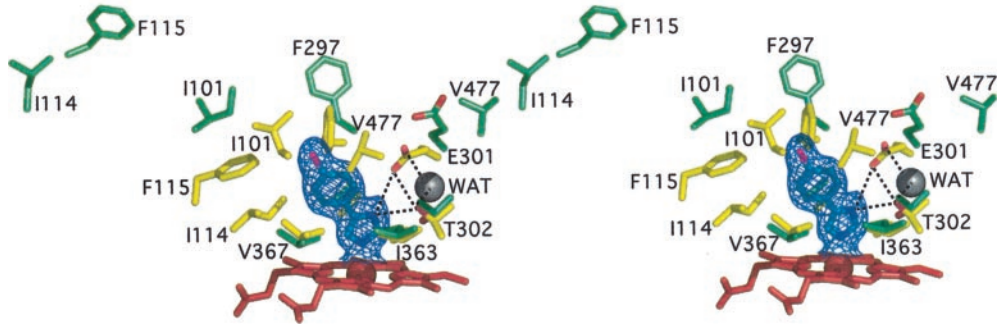

FIG. 6. **Changes in placement of active site residues shown in divergent (walleye) stereo.** Residues within a generous 5-Å contact distance from the inhibitor CPI are shown in stereo both at their positions in the 2B4/CPI complex (*yellow*) and in the open 2B4 conformation (*green*). The heme and CPI are shown as *red* and *cyan sticks*, respectively. A σ_A-weighted $2|F_o| - |F_c|$ electron density omit map is shown contoured at 1σ for CPI. The hydrogen-bonding network with the bound ligand is indicated by *dashed lines*. The following are the distances between a residue's closest atom to CPI in the 2B4/CPI complex and that atom's location in the open 2B4 conformation: Ile-101 (*I101*), 4.6 Å; Ile-114 (*I114*), 18.9 Å; Phe-115 (*F115*), 13.4 Å; Phe-297 (*F297*), 7.1 Å; Ala-298 (*A298*), 1.4 Å; Glu-301 (*E301*), 3.8 Å; Thr-302 (*T302*), 1.7 Å; Ile-363 (*I363*), 1.0 Å; Val-367 (*V367*), 0.6 Å; and Val-477 (*V477*), 12.3 Å.

electron density for CPI in the active site of 2B4 (Fig. 6). The molecule fits in a single orientation with an imidazole nitrogen coordinated to the heme iron at a bond distance of 2.14 Å. The long axis of CPI is at an angle of ~75° to the plane of the heme, leaning toward the B′ helix. The two CPI rings are not coplanar, with an angle of ~25° between them. The active site residues strictly constrain the inhibitor on all sides, such that nearly any rotation of the inhibitor would require a conformational change on the part of the protein. Residues within a generous contact distance of 5 Å from CPI represent SRSs 1, 4, 5, and 6. Residues Ile-101, Phe-115, and Val-477 interact most closely with the chlorine substituent. These residues, along with Ile-114, Phe-297, and Val-367, form a strongly hydrophobic environment surrounding the upper phenyl ring. The lower imidazole ring is circumscribed by Ala-298, Glu-301, Thr-302, and Ile-363, with the side chain oxygens of Glu-301 and Thr-302 forming a hydrogen-bonding network with the free nitrogen of the imidazole ring and a nearby water molecule. The complex is likely stabilized by this hydrogen bond between Glu-301 and CPI, which is possible because of protonation of the imidazole nitrogen at pH 4 during crystal growth. In contrast to the 2C5 structures with diclofenac and 4-methyl-*N*-methyl-*N*-(2-phenyl-2H-pyrazol-3-yl)benzenesulfonamide, no water molecules directly interact with the inhibitor.

Comparison of the 2B4 and 2B4/CPI structures reveals that contact residues flanking helix B′ (Ile-101, Ile-114, Phe-115, and SRS 1) and in the β_4 system (Val-477 and SRS 6) have the largest displacements, from 5 to 18 Å (Fig. 6), which are primarily a result of the repositioning of the protein backbone. More moderate differences observed in the placement of residues in helix I are largely derived from alterations in side chain conformation rather than the protein backbone. Residues in SRS 5 (Ile-363 and Val-367) are changed in their positions very little between the two 2B4 conformations.

Electron Transfer Face—The topography of the proximal side of the protein, which is implicated in NADPH cytochrome P450 reductase and cytochrome b_5 binding (26, 27), is significantly different between the two 2B4 structures, primarily as a result of differences in the placement of the C helix and the C/D loop (Fig. 5). The location of the C helix in the closed 2B4/CPI conformation most closely approximates the location of its counterpart observed in the crystal structure of the P450 BM-3 heme and the reductase FMN domain as well as in the closed structures of P450s from the 2C subfamily (Fig. 3*A*). In the open 2B4 conformation, a short loop directly connects helices C and D, but in the CPI complex the C/D region loops out away from the flanking helices, similar to the loop position in the 2C structures (Fig. 5). Portions of the C/D loop interact with residues in the G/H loop, causing a 4-Å shift in the backbone positions between the two 2B4 conformations. Interactions between the G/H and C/D loops may provide a physical mechanism for coordinating ligand-induced conformational changes on the distal side of the protein to electron delivery on the proximal side.

Heme Binding—In the 2B4/CPI complex, residues that interact with the heme propionate ring correspond to those performing this function in the closed forms of the 2C enzymes. Essentially, the A ring propionate is coordinated to Ser-430, His-369, and Arg-98, whereas the D ring also interacts with Arg-98 as well as with Arg-434, Arg-125, and Trp-121 (Fig. 7). This contrasts to the open conformation of 2B4, where Arg-434 and Arg-98 switch positions so that Arg-434 interacts with both propionates, whereas Arg-98 interacts only with the D ring propionate. Only the side chain of Arg-434 is repositioned to accomplish this switch, but both the backbone and the side chain of the B/C loop residue Arg-98 are relocated. A more significant change in the interactions with the D ring propionate occurs as the single interaction with Arg-133 in the open form is replaced by interactions with Trp-121 and Arg-125 in the closed CPI conformation. This change in heme binding is due to the relocation of the C helix that causes, for example, a 19.57-Å displacement of Trp-121 from a surface position in the open form to a buried position near the heme in the closed conformation.

DISCUSSION

CPI is the smallest ligand characterized to date in a mammalian P450 active site. The corresponding active site volume is far smaller than that of the structures of 2C enzymes, which contain substantial solvent in addition to the bound ligand. Although the structures of 2C5 with either diclofenac or 4-methyl-*N*-methyl-*N*-(2-phenyl-2H-pyrazol-3-yl)benzenesulfonamide identify 13 and 18 residues, respectively, within 5 Å of the bound ligand, only 10 residues are located within this distance from CPI in the 2B4/CPI complex. In contrast to the 2C5 structures, no waters or residues from the F, F′, G′, or G regions directly interact with CPI. In the 2B4/CPI complex, helix I (SRS 4) residues in contact with the inhibitor are limited to those immediately over the heme, whereas β_4 (SRS 6) contact residues are limited to Val-477 at the tip of the β-turn. The CPI contact residues at positions 114, 363, and 367 have been functionally implicated in the metabolism of steroids, 7-alkyoxyresorufins, 7-alkoxycoumarins, and benzphetamine (28) and seem to be part of the core active site for all of these substrates.

Site-directed mutagenesis of 2B enzymes has revealed that

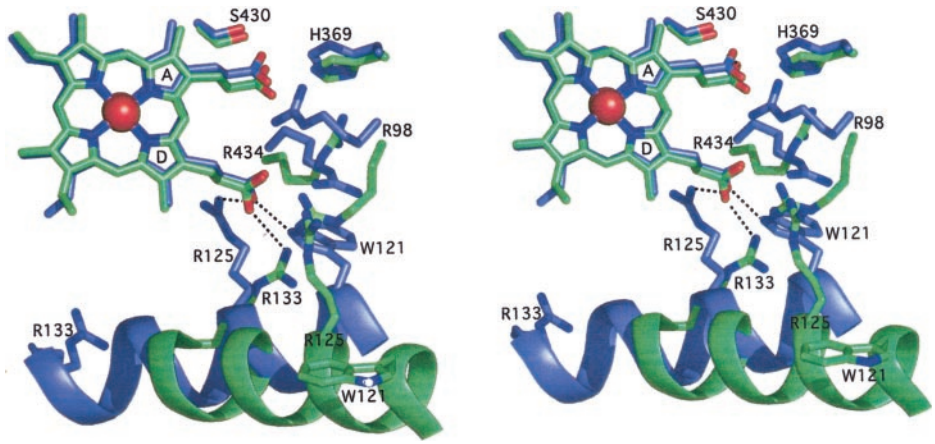

FIG. 7. **Changes in the position of the C helix and heme ligation upon CPI binding shown in divergent (walleye) stereo.** Residues in helix C (*ribbon*) alter positions significantly between the 2B4 open (*green*) and the CPI closed (*blue*) conformations, resulting in the loss of a hydrogen bond to the D ring propionate in the open conformation. Hydrogen bonds between the D ring propionate and helix C residues are indicated by *dashed lines*. Residues Arg-98 (*R98*), Ser-430 (*S430*), Arg-434 (*R434*), and His-369 (*H369*) have smaller changes in their positions and are labeled once near the base of the side chain.

the set of residues affecting metabolic regiospecificity and stereospecificity is substantially larger than that constituted by residues forming the CPI active site, suggesting an active site that adapts to substrates of different sizes and shapes. In particular, studies of 2B mutant enzymes with steroid substrates have suggested that ligand contact residues might also include those at positions 205, 206, 209, 219, 294, 362, 478, and 480 (see review in Ref. 28) (11, 29–33). These residues occur largely in the F/G region above the CPI active site or adjacent to CPI contact residues. Binding of larger ligands, such as steroids, would require substantial expansion of the active site volume and involve contact with a wider range of residues. The location of functionally important residues adjacent to CPI contact residues suggests a general expansion of the active site, whereas the role of F/G region residues suggests an orientation of the long axis of larger steroid substrates in this direction. Alternatively, functionally important residues that are not directly implicated in ligand contact could affect the energetic barrier between protein conformations and thus alter the ability of the protein to adopt a particular substrate binding orientation.

Although 2B4 and 2B5 are 97.5% identical, the difference in IC_{50} values for CPI between the two enzymes is almost 100-fold (23). Although most of the 12 amino acid differences are far from the active site, the I114F, I363V, and V367A substitutions are within 5 Å of CPI. With these substitutions, the milieu of hydrophobic residues surrounding CPI would be maintained in 2B5. However, replacement of Ile by Phe at position 114 in 2B5 would occlude significant volume on the B′/C side of the active site and impede CPI binding by steric hindrance. On the opposite side of the 2B5 active site, residues Val-363 and Ala-367 occupy less space than their respective Ile and Val counterparts in 2B4. Thus, although the active site volume may remain relatively unchanged between 2B4 and 2B5, the inhibitor or protein must assume relative orientations with significantly less favorable binding energy to the iron.

The entry of a ligand and the binding in the 2B4 active site appear to trigger the closing of the protein around the substrate. As a result, the overall structure of P450 2B4 complexed with the specific inhibitor CPI is largely reminiscent of the closed structures of cytochromes P450 from the 2C family that have been characterized recently (2, 6, 7, 24, 25). New interactions with the bound ligand in the closed form of 2B4 initiate conformational changes in helix B′, form the C-terminal turn of helix F, and relocate helices F′, G′, and G. Similar but smaller structural changes have been observed in structures of other mammalian and bacterial P450s. Structures of 2C5 with 4-methyl-N-methyl-N-(2-phenyl-2H-pyrazol-3-yl)benzenesulfonamide and diclofenac differ from each other mostly in the positions of the residues in helix B′ and the locations of helices F and G as a result of interactions with ligands of different sizes and shapes (6, 7). In addition, the region that includes helices F through G has the highest *B*-values in most P450 structures, suggesting flexibility. Although bacterial P450 structures do not have the short F′ and G′ helices, movement of the F/G loop away from the bulk protein, unraveling of the C-terminal turn of helix F, and repositioning of helices F and G have also been observed in liganded *versus* unliganded structures of the bacterial P450 119 (8, 9). The most significant difference between structures of the closely related bacterial P450s 154A1, obtained with a phenylimidazole inhibitor, and 154C1, obtained in an unliganded state, also involve repositioning of helices F and G (34). Overall, these results support the idea of a flexible P450 structure whose conformation is responsive to the presence of a ligand.

Comparison of the open and closed structures of 2B4 also suggests a structural mechanism for coordination of substrate binding and redox partner binding. In the 2B4 structures, the B′/C loop and the G/H loop, via interactions with the neighboring C/D loop, significantly alter the orientation of helix C. The positively charged residues on helix C play a key role in P450 interaction with redox partners (26). Thus, ligand binding on the distal side of the protein may partially mediate interaction with electron transfer partners on the proximal side. This is consistent with data showing that substrate binding both enhances reductase binding (35) and 2B4 reduction (36) over that of the substrate-free enzyme. The flexibility of helix I is also thought to be important in allowing diverse substrates to bind as well as in influencing redox partner binding (37) in at least some P450s.

The heme redox potential is known to be affected by many factors, including the proximal heme ligand and propionate and vinyl substituent orientations and interactions with the immediate protein environment. Both the crystal structure (38) and resonance Raman studies of BM3 (39) indicate that substrate binding produces a conformational change in one of the propionates, breaking a hydrogen bond interaction with the protein. Resonance Raman studies of 2B4 indicate that the addition of a substrate perturbs the heme-protein interaction in a substrate-dependent manner (40). The 2B4 structures indicate a net gain of a hydrogen bond to the D ring propionate upon conversion of the 2B4 open conformation to the CPI-bound closed conformation. These alterations in heme coordination may affect the heme redox potential. Such a structural link between substrate binding and the binding of redox partners would increase catalytic efficiency.

Although the open 2B4 structure is likely an exaggeration of the conformation required for entry of smaller substrates, it must be energetically accessible in solution. A comparison with the present closed structure yields insights into the dynamic structural elements of P450s that modulate both substrate

binding and redox partner binding and, thus, may at least partially coordinate catalysis. Because CPI is a relatively small ligand, these two 2B4 structures likely represent the extreme conformational changes available to P450s. These structures emphasize that the lid domain, active site, and redox partner binding interface are pliant, ligand-responsive structures. Consistent with recent structures of 2C5 with different bound ligands, functional evidence suggests that the contact residues identified in the 2B4/CPI complex likely represent a minimal set that would be expanded for larger ligands. Interactions with CPI promote a closed conformation whose structural rearrangements emanate via the B′ helix and the F/G region to relocate the C helix, thus likely affecting interaction with redox binding partners. Alterations in heme binding are coordinated with the relocation of helix C and may also affect redox potential and overall enzymatic activity. These same types of dynamics may exist on a smaller scale for intermediate protein conformations. The overall implications and the generality of the large scale conformational changes already observed for 2B4 are still under investigation but are consistent with smaller structural alterations observed for the thermophilic P450 119 (8, 9), and the bacterial P450 BM-3 (3).

Acknowledgments—We thank You Qun He for determining the activity of the H226Y mutant with 7-ethoxy-4-trifluoromethylcoumarin and Jason Yano, Vidyasankar Sundaresan, and the staff of the Advanced Light Source for data collection at that facility.

REFERENCES

1. Poulos, T. L., Finzel, B. C., and Howard, A. J. (1987) *J. Mol. Biol.* **195,** 687–700
2. Williams, P. A., Cosme, J., Sridhar, V., Johnson, E. F., and McRee, D. E. (2000) *Mol. Cell* **5,** 121–131
3. Haines, D. C., Tomchick, D. R., Machius, M., and Peterson, J. A. (2001) *Biochemistry* **40,** 13456–13465
4. Serbe, K., Pylypenko, O., Vitali, F., Zhang, W., Rouset, S., Heck, M., Vrijbloed, J. W., Bischoff, D., Bister, B., Sussmuth, R. D., Pelzer, S., Wohllenben, W., Robinson, J. A., and Schlichting, I. (2002) *J. Biol. Chem.* **277,** 47476–47485
5. Podust, L. M., Kim, Y., Arase, M., Neely, B. A., Beck, B. J., Bach, H., Sherman, D. H., Lamb, D. C., Kelly, S. L., and Waterman, M. R. (2003) *J. Biol. Chem.* **278,** 12214–12221
6. Wester, M. R., Johnson, E. F., Marques-Soares, C., Dansette, P., Mansuy, D., and Stout, C. D. (2003) *Biochemistry* **42,** 6370–6379
7. Wester, M. R., Johnson, E. F., Marques-Soares, C., Dijols, S., Dansette, P. M., Mansuy, D., and Stout, C. D. (2003) *Biochemistry* **42,** 9335–9345
8. Yano, J. K., Koo, L. S., Schuller, D. J., Li, H., Ortiz de Montellano, P. R., and Poulos, T. L. (2000) *J. Biol. Chem.* **275,** 31086–31092
9. Park, S. Y., Yamane, K., Adachi, S., Shiro, Y., Maves, S. A., Weiss, K. E., and Sligar, S. G. (2002) *J. Inorg. Biochem.* **91,** 491–501
10. Scott, E. E., He, Y. A., Wester, M. R., White, M. A., Chin, C. C., Halpert, J. R., Johnson, E. F., and Stout, C. D. (2003) *Proc. Natl. Acad. Sci. U. S. A.* **100,** 13196–13201
11. Scott, E. E., He, Y. Q., and Halpert, J. R. (2002) *Chem. Res. Toxicol.* **15,** 1407–1413
12. Otwinowski, Z. (1993) in *Proceedings of the CCP4 Study Weekend: Data Collection and Processing, Warrington, United Kingdom, January 29 and 30, 1993* (Sawyer, L., Isaacs, N., and Bailey, S., eds) pp. 56–62, Science and Engineering Research Council (SERC), Daresbury Laboratory, Warrington, UK
13. Leslie, A. G. W. (1994) *MOSFILM Users Guide*, Medical Research Council-Laboratory of Molecular Biology, Cambridge, UK
14. Collaborative Computing Project Number 4 (1994) *Acta Crystallogr. Sect. D Biol. Crystallogr.* **50,** 760–763
15. Terwilliger, T. C., and Berendzen, J. (1999) *Acta Crystallogr. Sect. D Biol. Crystallogr.* **55,** 849–861
16. Terwilliger, T. C. (2000) *Acta Crystallogr. Sect. D Biol. Crystallogr.* **56,** 965–972
17. van Aalten, D. M. F., Bywater, R., Findlay, J. B. C., Hendlick, M., Hooft, R. W. W., and Vriend, G. (1996) *J. Comput. Aided Mol. Des.* **10,** 255–262
18. Brunger, A. T., Adams, P. D., Clore, G. M., DeLano, W. L., Gros, P., Grosse-Kunsleve, R. W., Jiang, J. S., Kuszewski, J., Nilges, N., Pannu, N. S., Read, R. J., Rice, L. M., Simonson, T., and Warren, G. L. (1998) *Acta Crystallogr. Sect. D Biol. Crystallogr.* **64,** 905–921
19. Tickle, I. J., Laskowski, R. A., and Moss, D. S. (1998) *Acta Crystallogr. Sect. D Biol. Crystallogr.* **54,** 243–252
20. Matthews, B. W., and Czerwinski, E. W. (1975) *Acta Crystallogr. Sect. A* **31,** 480–487
21. McRee, D. E. (1999) *J. Struct. Biol.* **125,** 156–165
22. Laskowski, R. A., MacArthur, M. W., Moss, D. S., and Thornton, J. M. (1993) *J. Appl. Crystallogr.* **26,** 283–291
23. Spatzenegger, M., Wang, Q., He, Y. Q., Wester, M. R., Johnson, E. F., and Halpert, J. R. (2001) *Mol. Pharmacol.* **59,** 475–485
24. Schoch, G. A., Yano, J. K., Wester, M. R., Griffin, K. J., Stout, C. D., and Johnson, E. F. (2004) *J. Biol. Chem.* **279,** 9497–9503
25. Williams, P. A., Cosme, J., Ward, A., Angove, H. C., Matak-Vinkovic, D., and Jhoti, H. (2003) *Nature* **424,** 464–468
26. Bridges, A., Gruenke, L., Chang, Y. T., Vakser, I. A., Loew, G., and Waskell, L. (1998) *J. Biol. Chem.* **273,** 17036–17049
27. Lehnerer, M., Schulze, J., Achterhold, K., Lewis, D. F. V., and Hlavica, P. (2000) *J. Biochem.* **127,** 163–169
28. Domanski, T. L., and Halpert, J. R. (2001) *Curr. Drug Metab.* **2,** 117–137
29. Lin, H. L., Zhang, H., Waskell, L., and Hollenberg, P. F. (2003) *J. Pharmacol. Exp. Ther.* **306,** 744–751
30. Harlow, G. R., and Halpert, J. R. (1996) *Arch. Bioch. Biophys.* **326,** 85–92
31. Hasler, J. A., Harlow, G. R., Szklarz, G. D., John, G. H., Kedzie, K. M., Burnett, V. L., He, Y., Kaminsky, L. S., and Halpert, J. R. (1994) *Mol. Pharmacol.* **46,** 338–345
32. Domanski, T. L., He, Y. Q., Scott, E. E., Wang, Q., and Halpert, J. R. (2001) *Arch. Biochem. Biophys.* **394,** 21–28
33. Szklarz, G. D., He, Y. A., and Halpert, J. R. (1995) *Biochemistry* **34,** 14312–14322
34. Podust, L. M., Bach, H., Kim, Y., Lamb, D. C., Arase, M., Sherman, D. H., Kelly, S. L., and Waterman, M. R. (2003) *Protein Sci.* **13,** 255–268
35. Reed, J. R., and Hollenberg, P. F. (2003) *J. Inorg. Biochem.* **97,** 276–286
36. Kanaeva, I. P., Nikityuk, O. V., Davydov, D. R., Dedinskii, I. R., Koen, Y. M., Kuznetsova, G. P., Skotselyas, E. D., Bachmanova, G. I., and Archakov, A. I. (1992) *Arch. Bioch. Biophys.* **298,** 403–412
37. Podust, L. M., Poulos, T. L., and Waterman, M. R. (2001) *Proc. Natl. Acad. Sci. U. S. A.* **98,** 3068–3073
38. Li, H., and Poulos, T. L. (1997) *Nat. Struct. Biol.* **4,** 140–146
39. Chen, Z., Ost, T. W. B., and Schelvis, J. P. M. (2004) *Biochemistry* **43,** 1798–1808
40. Macdonald, I. D. G., Smith, G. C. M., Wolf, C. R., and Smith, W. E. (1996) *Biochem. Biophys. Res. Comm.* **226,** 51–58
41. Delano, W. L. (2002) *The PyMOL User's Manual*, Delano Scientific, San Carlos, CA
42. Guex, N., and Peitsch, M. C. (1997) *Electrophoresis* **18,** 2714–2723